Chemical order in Ga or Sb modified germanium sulfide glasses around stoichiometry: high-resolution XPS and Raman studies

R. Golovchak[a*], V. Nazabal[b], B. Bureau[b], J. Oelgoetz[a], A. Kovalskiy[a], H. Jain[c]

[a]*Department of Physics, Engineering and Astronomy, Austin Peay State University, Clarksville, TN 37044, USA*
[b]*Equipe Verres et Céramiques, UMR-CNRS 6226, Université de Rennes 1 35042 Rennes Cedex, FRANCE*
[c]*Department of Materials Science and Engineering, Lehigh University, 5 East Packer Avenue, Bethlehem, PA 18015-3195, USA*

Abstract

To understand the unique features of germanium sulfide (~60-70 at.% of S) glasses modified with Ga or Sb, the chemical order in these materials is investigated using X-ray photoelectron spectroscopy (XPS). The obtained results are correlated with Raman spectroscopy data and verified with quantum chemical calculations. It is shown that in addition to the regular corner-shared and S-S-shared [$SbS_{3/2}$] pyramids and [$GeS_{4/2}$] tetrahedra, a fraction of these structural units can form edge-shared fragments. The obtained XPS results also support the possibility for [$SbS_{5/2}$] distorted square pyramids formation in Sb-rich glasses. At higher concentrations of antimony, a tendency to the increased concentration of homopolar bonds is observed.

Keywords: chalcogenide glass, electronic and atomic structure, XPS

*Corresponding author. Tel.: +1 931 221 6361
E-mail address: holovchakr@apsu.edu (R. Golovchak)

Introduction

Binary and ternary sulfide glasses based on arsenic, germanium or antimony have been recently proposed for numerous applications in modern photonics [1-3]. Many of the proposed ternary compositions contain ~60-70 at.% sulfur and 15-25 at.% Ge. For example, $Ge_{15}As_{15}S_{70}$ glass shows an ultrafast optical switching effect [4], and $Ge_{23}Sb_7S_{70}$ composition has been proposed for planar and 3D waveguides [5] and glass-on-graphene photonics [6]. The rare-earth doped $Ge_{25}Ga_5S_{70}$ glass has been shown to be suitable for optical fibers and amplifiers [7], and Ga_2S_3 modified $Ge_{33}S_{67}$ glasses has been proposed for use in solid state lithium batteries [8]. These compositions, as a rule, were established empirically by searching for optimal physical properties of interest within the corresponding tie-lines of glass-forming regions. The structural aspects of such compositions have remained poorly understood, mostly because there are very few experimental techniques capable of providing unambiguous information about the structure of ternary glasses. Traditional vibrational spectroscopy techniques alone, such as IR or Raman spectroscopies, are not as helpful as in the case of binary compounds, because of a much greater variety of structural units, which leads to a considerably higher number of possible vibrational modes with overlapping contributions to the IR or Raman spectrum [9,10]. Structural interpretation of the obtained spectra is, therefore, often ambiguous. Conventional NMR methods are also difficult to apply to chalcogenides because of the both the low abundance of NMR-active chalcogen isotopes (low abundance means long data collection times) and comparable magnitudes of chemical shifts for different cation-centered structural units.[11,12]. Thus, in our view, one of the most informative technique to determine the structure of ternary chalcogenide glasses is the high-resolution X-ray photoelectron spectroscopy (XPS). This method has been successfully used to explain structural development in various binary and ternary glasses (e.g.

As-Se, Ge-Se, As-S, Ge-S, As-Ge-Se, Ga-Ge-Se and Ge-Sb-Se) [13-20]. It allowed not only to identify the main building blocks in these glass networks, but also to quantify their moieties and relative concentrations. Thus far, systematic high-resolution XPS studies have not been performed for ternary Ge-S based glasses.

Since most of the glasses suitable for practical applications in photonics contain ~60-70 at.% of sulfur and a considerable concentration of Ge [1-8], we decided to start with $Ge_{33}S_{67}$ stoichiometric glass as reference and add Ga ($Ge_{25}Ga_5S_{70}$) or Sb ($Ge_{25}Sb_5S_{70}$, $Ge_{25}Sb_{10}S_{65}$ and $Ge_{20}Sb_{15}S_{65}$), forming compositions relatively rich in sulfur or stoichiometric. This allowed us to explore the glass network formation in Ge-S matrix when it is perturbed by atoms with comparable to Ge size but variable coordination number (Ga can deviate from known "8-N" rule, being 4-fold coordinated in many chalcogenide glass matrices) [19,20] or larger atoms but with well-defined coordination (Sb is known to obey the "8-N" rule in sulfide glass networks, having coordination 3 in non-defect state) [18,20,21]. The analysis of chemical order is built on our previous XPS studies in binary Ge-S as well as a number of ternary Ge, Ga and Sb-containing glasses [14-16,18,19,21]. The assignment of XPS peaks is supported by theoretical calculations and Raman spectra analysis.

Experimental

The $Ge_{33}S_{67}$, $Ge_{25}Ga_5S_{70}$, $Ge_{25}Sb_5S_{70}$, $Ge_{25}Sb_{10}S_{65}$ and $Ge_{20}Sb_{15}S_{65}$ glasses were prepared by the conventional melt-quench method from a mixture of high-purity elemental germanium, gallium, antimony and sulfur purified by distillation. The sealed silica ampoules were slowly heated and homogenized in a rocking furnace for 12 h at high temperature (800 °C to 1000 °C) chosen according to the composition of the glass. Then, the ampoules with melt were quenched in air or into the water, and annealed 20 °C below glass transition temperatures (T_g ~ 490 °C for $Ge_{33}S_{67}$, T_g ~ 340 °C for $Ge_{25}Ga_5S_{70}$, T_g ~ 300 °C for $Ge_{25}Sb_5S_{70}$, T_g ~ 360 °C for $Ge_{25}Sb_{10}S_{65}$ and T_g ~ 280 °C for $Ge_{20}Sb_{15}S_{65}$ glasses) to relieve the mechanical strains. Nominal compositions of the prepared glasses were confirmed by the XPS core levels ratio analysis.

High resolution XPS spectra were recorded with a Scienta ESCA-300 spectrometer using monochromatic Al K_α X-rays (1486.6 eV) under a vacuum of 2×10^{-8} Torr (or less), as described elsewhere [14-18]. To obtain structural information about the bulk of glass, the samples were cleaved directly in the ultrahigh-vacuum chamber of the spectrometer and the data were collected from these freshly fractured surfaces. The surface charging from photoelectron emission was neutralized using a low energy (<10 eV) electron flood gun. The experimental positions of the core levels were adjusted by referencing to the position of 1s core level peak (284.6 eV) of adventitious carbon [22]. XPS data were analyzed with standard CASA-XPS software package, using Shirley background and a pseudo-Voigt line shape for the core level peaks [23]. The pseudo-Voigt function was approximated by Gaussian/Lorentzian product form, where the mixing was fixed to be 0.3 (0 is a pure Gaussian, 1 is a pure Lorentzian) for all doublets of the analyzed core-levels. The 3*d* core-level XPS spectra of Ga and Ge, 4*d* core-level XPS spectra of Sb and 2*p* core-level XPS spectra of S were used for quantitative analysis of chemical order in the investigated glasses. The number of doublets (which consisted of $d_{5/2}$ and $d_{3/2}$, or $p_{3/2}$ and $p_{1/2}$ components owing to spin-orbit splitting) within a given peak was determined by an iterative curve fitting procedure in which a doublet was added only if it significantly improved the goodness of the fit. The parameters used to link the $d_{5/2}$ and $d_{3/2}$ components were: a peak separation of 0.46 eV for Ga, 0.56 eV for Ge, 1.24 eV for Sb, and an area ratio 1.45 for all doublets of *d* core levels. For the *p* core level of S, the peak separation was taken to be 1.16 eV and a $p_{3/2}/p_{1/2}$ peak area ratio of 2 was used. The full width at half maximum (*fwhm*) was assumed to be the same for the peaks within a given doublet, but different *fwhm* values were allowed for independent doublets of the same core-level peak. With these constraints, the uncertainties in the peak position (binding energy, BE) and area (*A*) of each component were ± 0.05 eV and ± 2 % respectively.

In order to explore the thermochemistry of the possible structural transitions of interest, calculations for a number of sample molecules were carried out using the Density Functional Theory in Gaussian 09 software [24] package, using the B3LYP density functional [25-29] and the Def2-QZVPPD basis set [30] (with the associated effective core potential on the Sb atoms [31]) as retrieved from the EMSL basis set library [32,33]. Vibrational modes were treated as harmonic oscillators. The molecules were chosen to represent face-shared (each metal shares 3 sulfurs with its neighbor), edge-shared (each metal shares 2 sulfurs with its neighbor) and corner-shared (each metal atom shares a sulfur with its neighbor) as well as configurations with a metal-metal bond and the metals connected through a pair of sulfurs (dimer). Hydrogens were added, where needed, to terminate the fragments at the sites of their connection with the rest of covalent network. Thermochemical calculations were carried out by Gaussian 09 following the standard treatment laid out in Ref. [34]. We expect the uncertainties in these calculations to be no less than about 5×10^{-20} J (a few cal/mol). It should be noted that we chose a temperature of 25 °C for the thermochemical calculations because of the limitations of the harmonic oscillator approximation. At the quenching temperatures for these glasses, we expect highly excited vibrational states to be important to the partition function, thus we recognize that approximating the vibrational modes as harmonic oscillators may not be adequate. Nevertheless, such low-temperature calculations are still relevant, because if a fragment could exist at colder temperatures, it is even more likely to be present in a sample with an effective temperature close to the quenching temperature.

Raman spectra were collected using LabRam HR800 (Horiba Jobin-Yvon) spectrometer at room temperature using 785 nm laser excitation. To avoid possible photoinduced changes, the power of the laser was reduced with optical density filters and did not exceed 1 mW.

Results and discussion

XPS survey spectra of the investigated samples show well defined core level peaks of constituent chemical elements and the related Auger lines identified using the reference spectra in the PHI handbook [22]. There was no evidence for a significant concentration of the impurities (oxygen-based complexes being most likely) in the investigated glasses and their compositions were found to be close to the nominal value.

The analysis of chemical order can be accomplished through the quantification of core-level XPS spectra, as was shown for many other chalcogenide glass systems [13-19,35,36]. It is based on the difference in electronegativity of constituent atoms, which introduces chemical shifts in the XPS peaks corresponding to different structural fragments. This shift is due to the difference in the electron density distribution, determined by the oxidation state and coordination of the probed element and its neighbors. Therefore, each separate doublet appearing in the fit of the experimental XPS core level spectrum would correspond to a specific chemical environment (structural fragment) of the probed element and its electronic configuration. As a rule, the higher is the electronegativity value of the neighbors in a structural fragment or the oxidation number/coordination of the probed element, the greater would be a shift of corresponding doublet to higher binding energy values [13-19]. Thus, a number of doublets in the fit gives a number of possible chemical environments for the absorbing atom, whereas the area under each doublet gives the concentration of the associated moiety. The difference in electronegativity of the constituent chemical elements (χ_{Ga}=1.81, χ_{Ge}=2.01, χ_{Sb}=2.05, χ_{S}=2.58) [37] allows us to unambiguously distinguish between chalcogen and cation environment of the probed element.

According to our previous investigations of the Ge-S binary glass system [16], the observed doublet with a primary ($d_{5/2}$) component at ~30.9 eV in Ge 3*d* core level XPS spectrum (Table 1, Fig. 1) can be associated with corner-shared (CS) [$GeS_{4/2}$] tetrahedra. Existence of another high-BE doublet with primary component at ~31.4 eV (Table 1, Fig. 1), the most probably, is caused by the edge-shared (ES) [$GeS_{4/2}$] tetrahedra, as it was suggested previously for Ge-Se and Ge-S glasses [14,16]. Then, the low-BE doublet at ~30.1-30.5 eV in Ge 3*d* core level XPS spectra (Table 1, Fig. 1) should be associated with a substitution of S in [$GeS_{4/2}$] complexes by Ge or Sb. In $Ge_{25}Ga_{5}S_{70}$ glass, this doublet is even more shifted toward low-BE side of Ge 3*d* core level spectrum (observed at ~29.7 eV with ~2% moiety), which may be due to the formation of small concentration of Ge-Ga bonds (Ga has the lowest electronegativity value [37]) or 3-fold coordinated Ge atoms although for this composition, which is relatively rich in sulfur, the probability is relatively low. The Ga 3*d* core level XPS spectrum, on the other hand, can be fitted by two doublets (Fig. 1) with primary components at ~19.8 eV and 19.5 eV both having *fwhm* ~0.9 eV (Table 2). Position of the first doublet agrees well with BE of Ga 3*d* electrons in sulfur surrounding (19.8 eV) [38], while the second doublet on low-BE side may indicate the presence of Ga-Ga or Ga-Ge bonds (ethane-like units) when at least one sulfur atom in [$GaS_{4/2}$] unit is replaced by Ga or Ge. The possibility of such units formation is also shown in S-deficit GeS_2-Ga_2S_3 glasses by theoretical calculations and Raman studies [39,40].

The Sb-containing glasses show a clear tendency to an increase in the area of low-BE doublet of Ge 3*d* core level spectra with increasing Sb concentration (Table 1), which can be well explained by the increase in the concentration of Ge-cation bonds (like Ge-Ge or Ge-Sb bonds) even if the composition are still rich in Sulfur or stoichiometric. Nevertheless, the maximum concentration of Ge-cation (**Ge**-Ge, **Ge**-Ga and **Ge**-Sb) bonds, as estimated from the moieties of corresponding fragments in Tables 1-3, does not exceed 5 % of total covalent bonds. In other words, formation of heteropolar cation-S bonds is strongly preferred.

When Sb content is low (< 10 at.%), most of the Sb atoms form [$SbS_{3/2}$] pyramids, which give rise to the XPS peak at ~33.2 eV (Table 2) [41]. Increase in the Sb concentration to 10 at.% and beyond leads to the appearance of two additional doublets in Sb 4*d* core level spectra (Fig. 1) with primary components at ~34.0 eV and ~32.1 eV (Table 2). The low-BE doublet is consistent with the formation of cation-cation (**Sb**-Ge, **Sb**-Sb) bonds within [$SbS_{3/2}$] pyramid (≤5%). If more than one S atom is substituted in [$SbS_{3/2}$] pyramid, a greater low-BE chemical shift is expected, which can be the reason for the lower position of this doublet in $Ge_{20}Sb_{15}S_{65}$ glass than in $Ge_{25}Sb_{10}S_{65}$ glass (Table 2). For the high-BE doublet with primary component at ~34.0 eV, we have to assume either the formation of positively charged over-coordinated Sb defects (which is doubtful due to high metallicity of Sb bonds [21]), formation of [$SbS_{3/2}$] pyramids that are edge-sharing with each other or with [$GeS_{4/2}$] tetrahedra, or [$SbS_{5/2}$] distorted square pyramids with the Sb atom slightly below the base center (the interatomic Sb-S distances being 2.46, 2.68, 2.68, 2.85 and 2.85 Å) [42,43]. The possibility for edge-sharing of [$SbS_{3/2}$] pyramids looks attractive, especially owing to the existence of such structural entities in stibnite (Sb_2S_3 mineral) [44]. However, the observed shift of corresponded doublet to the high-BE end is about ~0.8 eV (Table 2), which is a bit too high for a just change in a type of connection between structural units (for comparison, the difference between ES and CS $GeS_{4/2}$ tetrahedra is at most ~0.5 eV, see Table 1). So, the possibility of [$SbS_{5/2}$] distorted square pyramids formation of about 10% in the investigated glasses looks also plausible from the obtained XPS data.

The analysis of S 2*p* core level XPS spectra (Fig. 2) shows that stoichiometric $Ge_{33}S_{67}$ glass does contain a small amount of S-S bonds (doublet with primary component at ~162.2 eV, Table 3), whereas most of the S atoms (96 %) participate in the Ge-**S**-Ge (the probed atom in a moiety is shown in bold font) linkage responsible for the doublet with a primary component at ~161.7 eV [16]. Statistics of S-**S**-Ge and Ge-**S**-Ge complexes in $Ge_{25}Ga_5S_{70}$ glass (Table 3) roughly correspond to the statistics determined for Ge chalcogenides with 70 at.% chalcogen [14]. The doublet with primary component at 160.3 eV is most probably due to Ga-**S**-Ga fragments owing to the lowest electronegativity of Ga. When 5 at.% of Sb is introduced in place of Ga, the number of S-S linked structural units increases, as can be concluded from the increased contribution of the doublet at ~161.9 eV (Table 3). Such behavior is expected, if we assume that 4-fold coordinated Ga in $Ge_{25}Ga_5S_{70}$ glass (which is usually the case in chalcogenide matrixes [19]) is substituted with 3-fold coordinated Sb, which should make more S atoms available for the backbone if everything else being equal, especially the proportion of M-M bond (M = Ge, Ga, Sb). An additional doublet with primary component at 163.1 eV and relatively small intensity (relative area, *A*~4%) also appears on the high-BE end of S 2p core level spectrum of $Ge_{25}Sb_5S_{70}$ glass. It can be associated with S-**S**-S complexes on the basis of our previous studies [16]. It can be also attributed to 3-fold coordinated sulfur or S participating in [$SbS_{5/2}$] units, if the formation of the latter is assumed. A further increase in Sb concentration at the expense of S leads to almost complete disappearance of S-S bridges in $Ge_{25}Sb_{10}S_{65}$ and

$Ge_{20}Sb_{15}S_{65}$ glasses (Table 3) while the component at 163.1eV remains (S-**S**-S, 3-fold coordinated sulfur and/or presence of $[SbS_{5/2}]$).

In general, Raman spectra of the investigated glasses (Fig. 3) support the XPS analysis. The low frequency complex band at ~250-280 cm^{-1} is due to $(S)_3$-Ga-Ga(Ge)-$(S)_3$ ethane-like structural units [39], which are clearly observed only in $Ge_{25}Ga_5S_{70}$ glass. The edge-shared $[GeS_{4/2}]$ tetrahedra (ES-$[GeS_{4/2}]$) have their signatures at 372 cm^{-1} (A_{1C} symmetric mode) and 436 cm^{-1} in GeS_2–rich glass [39], while the A_1 symmetric breathing mode of corner-shared tetrahedra (CS-$[GeS_{4/2}]$) should contribute to the band at 344 cm^{-1} [39]. We believe the broad feature observed in the Raman spectra in the 400-450 cm^{-1} range (Fig. 3) testifies to the presence of some ES-$[GeS_{4/2}]$ tetrahedra in all of the investigated glasses. However, strong overlap with other vibrational modes in that region (not shown in Fig. 3) makes it almost impossible to quantify the concentration of ES vs CS units from Raman spectra alone. On the other hand, the concentration of ES units obtained from XPS analysis (Table 1 and Table 2) includes also mixed ES pyramids and tetrahedra, which have different Raman signatures. Therefore, both techniques must be used in a complementary fashion to determine the type of ES structural units. The -S-S- bridge stretching vibrations give rise to a band centered at 475 cm^{-1} [45], which is well observed in Raman spectra of $Ge_{25}Ga_5S_{70}$ and $Ge_{25}Sb_5S_{70}$ samples with most -S-S- content, as also found from XPS analysis (Table 3). The increase in Sb concentration leads to an increase in the intensity of bands at 290 cm^{-1} and 314 cm^{-1}, which are associated with E and A_1 vibrational modes of $[SbS_{3/2}]$ pyramids [9,45]. The vibrational modes corresponding to $(S)_3$-Ge-Ge-$(S)_3$ ethane-like and $(S)_3$-Ge-Sb-$(S)_2$ structural units, which are expected in all Sb-containing compositions according to the XPS analysis (Table 1), are hardly observed in the experimental Raman spectra (specifically in 200-300 cm^{-1} range) due to their lower Raman activity and low concentration (not exceeding 13 at.% of Ge sites for both fragments, see Table 1) compare to those of regular CS or ES units, in good agreement with other Raman data on glassy germanium sulfides [46,47]. Therefore, Raman spectroscopy could be not a very useful tool in the determination of low Ge-Ge homopolar bond concentration (<10%). On the other hand, XPS analysis tends to overestimate slightly the proportion of M-M bonds.

To verify the possibilities of edge- and corner sharing, we have performed quantum-chemical calculations for a number of possible configurations of neighbored pyramidal ([$SbS_{3/2}$] and [$GaS_{3/2}$]) and tetrahedral [$GeS_{4/2}$] structural units. The ES and FS units based on 3-fold coordinated Ga are used for comparison only, since we expect all our Ga atoms to be 4-fold coordinated in the considered glass network. The change in each energy is calculated in the usual way, namely (products) – (reactants), and summarized in Tables 4 and 5. The reactions 4.1-4.6 (Table 4) wherein a face-shared (FS) molecule (such as Sb_2S_3) reacts with SH_2 to produce an ES structure (such as $Sb_2S_4H_2$) are all exothermic (as indicated by $\Delta E < 0$) and can occur spontaneously at 25 °C ($\Delta G < 0$). The reactions 5.1-5.6 when ES structural units (like $Sb_2S_4H_2$) switches to CS (like $Sb_2S_5H_4$) are also exothermic, but with much smaller gain in the energies (Table 5). Moreover, they are unlikely to occur spontaneously at 25 °C, since $\Delta G > 0$. It means, that if ES units are formed during the synthesis (quenching) they would persist at room temperature.

According to the performed calculations, the most energetically favorable configurations are CS structural units (pyramids and/or tetrahedra) and the most energetically unfavorable are the FS units. The latter are included for comparison purposes only, since no FS units are expected in the structure of the investigated glasses according to the XPS analysis. The difference between ES and CS configurations is not as large as the difference between them and

FS configurations (Tables 4,5). So, we may expect formation of ES configurations too, though in a lower concentration than CS. This conclusion is in good agreement with the statistics of structural fragments determined through the moieties of observed doublets in the XPS core level spectra (Tables 1,2). The performed calculations also allow the prediction of the vibrational modes, their position (within 5 % accuracy) and Raman activity for the ES and CS structural fragments. Although the positions of these modes (the strongest are shown by arrows in Fig. 3) are approximate, their overlap with experimental Raman spectra supports the idea about the presence of both CS and ES structural fragments in the investigated glasses.

The possibilities for metal-metal bonds and -S-S- bridges formation are evaluated on the basis of similar calculations, and the results are presented in Table 6. Accordingly, the formation of Sb-Sb bonds is preferred over Ge-Ge bonds (Table 6, reaction 6.1) and Ge-Sb bonds (Table 6, reaction 6.2). The formation of Ge-Ge bonds and Ge-Sb bonds is almost equally likely based on the values of enthalpy of formation, giving slight preference to the latter ones (Table 6, reaction 6.3). That is why even at small Sb concentration it is possible to observe Sb-metal bonds with XPS (Table 2). The simultaneous existence of Sb-Sb, Ge-Ge or Ge-Sb bonds with S-S bonds (Table 6, reactions 6.4-6.7) is not energetically favorable compared to the regular CS structural units. In other words, chalcogen-metal bonds are strongly preferred in the investigated ChG, which is fully consistent with the observed low concentration of metal-metal bonds in the XPS spectra of the investigated glasses (Tables 1,2). However, if over-stoichiometric S-S bridges are formed, it would rather exist between two Sb atoms than between two Ge, or Ge and Sb atoms (Table 6, reactions 6.8-6.9).

Conclusions

From the analysis of Ga, Ge, Sb and S core level XPS spectra, we conclude that a higher concentration of Sb likely stimulates phase separation processes in the form of S-rich fragments and units containing metal-metal bonds. Part of the [$SbS_{3/2}$] pyramids might exist in edge-shared configurations either with each other or with tetrahedral structural units, increasing also the apparent number of edge-shared [$GeS_{4/2}$] tetrahedra, as can be deduced from high-BE fits of XPS spectra. Alternatively, high-BE doublet in Sb 4*d* core level XPS spectra can be associated with a formation of [$SbS_{5/2}$] distorted square pyramids found in some crystalline counterparts. The trends of metal-metal bond formation and subsequent phase separation processes can explain why no more than 15 at.% of Sb is found in most compositions suitable for practical applications. The quantum-chemical calculations show a strong preference for metal-chalcogen bonds, whereas the formation of "wrong" metal-metal and S-S bonds is most probably driven by steric inconsistencies between pyramidal and tetrahedral structural units, which impose geometric constraints on a larger scale than the performed calculations. Raman spectroscopy fully supports the assignment of doublets in Ge, Sb and S core level XPS peaks, including also Ga-Ga(Ge) bonds in $Ge_{25}Ga_5S_{70}$ glass.

Acknowledgments

The authors thank U.S. National Science Foundation, through International Materials Institute for New Functionality in Glass (Grant No. DMR-0844014), for initiating the international collaboration and providing financial support for this work. The group from Austin Peay State University acknowledges financial support from NSF Grant DMR-1409160 and TN Spacegrant Consortium. Calculations were run on APSU's cluster, which was acquired under

NSF Grant CNS-0722890. The authors would like to thank also Dr. Henry Luftman from Lehigh University for help with XPS measurements.

References

[1] B. J. Eggleton, B. Luther-Davies, K. Richardson, Chalcogenide Photonics, Nature Photonics 5 (2011) 141–148.

[2] J-L. Adam and X. Zhang (Ed.), Chalcogenide Glasses: Preparation, Properties and Application, Woodhead Publishing series in Electronic and Optical Materials No.44, 2014.

[3] X. Zhang, B. Bureau, P. Lucas, C. Boussard-Pledel, J. Lucas, Glasses for Seeing Beyond Visible. Chem. Eur. J. 14 (2008) 432-442.

[4] C. D'Amico, C. Caillaud, P. K. Velpula, M. K Bhuyan, M. Somayaji, J.-P. Colombier, J. Troles, L. Calvez, V. Nazabal, A. Boukenter, R. Stoian, Ultrafast Laser-Induced Refractive Index Changes in $Ge_{15}As_{15}S_{70}$ Chalcogenide Glass, Optical Materials Express 6 (2016) 1915-1928.

[5] H. Lin, L. Li, Y. Zou, O. Ogbuu, S. Danto, J.D. Musgraves, K. Richardson, J. Hu, Chalcogenide Glass Planar Photonics: from Mid-IR Sensing to 3-D Flexible Substrate Integration, Proc. SPIE 8600, Laser Resonators, Microresonators, and Beam Control XV 2013, 86000K. doi:10.1117/12.2000683.

[6] H. Lin, Y. Song, Y. Huang, D. Kita, S. Deckoff-Jones, K. Wang, L. Li, J. Li, H. Zheng, Zh. Luo, H. Wang, S. Novak, A. Yadav, Ch. Huang, R.-J. Shiue, D. Englund, T. Gu, D. Hewak, K. Richardson, J. Kong, J. Hu, Chalcogenide Glass-on-Graphen Photonics, Nature: photonics 11 (2017) 798–805.

[7] K. Wei, D.P. Machewirth, J. Wenzel, E. Snitzer, G.H. Sigel, Pr^{3+}-doped Ge-Ga-S Glasses for 1.3 μM Optical Fiber Amplifiers, J. Non-Cryst. Solids 182 (1995) 257-261.

[8] J. Saienga, Y. Kim, B. Campbell, S.W. Martin, Preparation and Characterization of Glasses in the $LiI+Li_2S+GeS_2+Ga_2S_3$ System, Solid State Ionics 176 (2005) 1229–1236.

[9] L. Petit, N. Carlie, F. Adamietz, M. Couzi, V. Rodriguez, K.C. Richardson, Correlation Between Physical, Optical and Structural Properties of Sulfide Glasses in the System Ge–Sb–S, Mater. Chem. Phys. 97 (2006) 64-70.

[10] V. Nazabal, F. Charpentier, J.-L. Adam, P. Nemec, H. Lhermite, M.-L. Brandily-Anne, J. Charrier, J.-P. Guin, A. Moréac, Sputtering and Pulsed Laser Deposition for Near- and Mid-Infrared Applications: A Comparative Study of $Ge_{25}Sb_{10}S_{65}$ and $Ge_{25}Sb_{10}Se_{65}$ Amorphous Thin Films, Int. J. Appl. Ceram. Tec. 8 (2011) 990-1000.

[11] H. Eckert, J.P. Yesinowski, Sulfur-33 NMR At Natural Abundance In Solids. J. Am. Chem. Soc., 108, *9* (1986) 2140–2146.

[12] B. Bureau, J. Troles, M. Le Floch, P. Guenot, F. Smektala, J. Lucas, Germanium Selenide Glass Structures Studied by ^{77}Se Solid State NMR and Mass Spectroscopy, J. Non-Cryst. Solids 319 (2003) 145-153.

[13] R. Golovchak, A. Kovalskiy, A.C. Miller, H. Jain, O. Shpotyuk, The Structure of Se-Rich As-Se Glasses by High-Resolution X-Ray Photoelectron Spectroscopy, Phys. Rev. B 76 2007) 125208 (7).

[14] R. Golovchak, O. Shpotyuk, S. Kozyukhin, A. Kovalskiy, A.C. Miller, H. Jain, Structural Paradigm of Se-Rich Ge-Se Glasses by High-Resolution X-Ray Photoelectron Spectroscopy, J. Appl. Physics 105 (2009) 103704 (7).

[15] R. Golovchak, O. Shpotyuk, J.S. McCloy, B.J. Riley, C.F. Windisch, S.K. Sundaram, A. Kovalskiy, H. Jain, Structural Model of Homogeneous As-S Glasses Derived from Raman Spectroscopy and High-Resolution XPS, Phil. Magazine 90 (2010) 4489–4501.

[16] R. Golovchak, O. Shpotyuk, S. Kozyukhin, M. Shpotyuk, A. Kovalskiy, H. Jain, Short-Range Order Evolution in S-Rich Ge-S Glasses by X-Ray Photoelectron Spectroscopy, J. Non-Cryst. Solids 357 (2011) 1797-1803.

[17] R. Golovchak, O. Shpotyuk, M. Iovu, A. Kovalskiy, H. Jain, Topology and Chemical Order in $As_xGe_xSe_{1-2x}$ Glasses: A High-Resolution X-Ray Photoelectron Spectroscopy Study, J. Non-Cryst. Solids 357 (2011) 3454-3460.

[18] D. Sati, A. Kovalskiy, R. Golovchak, H. Jain, Structure of $Sb_xGe_{40-x}Se_{60}$ Glasses around 2.67 Average Coordination Number, J. Non-Cryst. Solids 358 (2012) 163-167.

[19] R. Golovchak, L. Calvez, E. Petracovschi, B. Bureau, D. Savitskii, H. Jain, Incorporation of Ga into the Structure of Ge-Se Glasses, Materials Chem. & Physics 138 (2013) 909-916.

[20] A. Feltz, Amorphous Inorganic Materials and Glasses; VCH, Weinheim, 1993.

[21] A.P. Kovalskiy, H. Jain, A.C. Miller, R.Ya. Golovchak, O.I. Shpotyuk, A Study of Reversible γ-Induced Structural Transformations in Vitreous $Ge_{23.5}Sb_{11.8}S_{64.7}$ by High-Resolution X-Ray Photoelectron Spectroscopy, J. Phys. Chem. B 110 (2006) 22930-22934.

[22] J.F. Moulder, W.F. Stickle, P.E. Sobol, K.D. Bomben, Handbook of X-ray Photoelectron Spectroscopy / Ed. J. Chastein. Perkin-Elmer Corp., Phys. Electr. Div., Eden Prairie, Minnesota, 1992.

[23] J.D. Conny, C.J. Powell, Standard Test Data For Estimating Peak Parameter Errors in X-Ray Photoelectron Spectroscopy, Surf. Interface Anal. 29 (2000) 856-872.

[24] M. J. Frisch, G. W. Trucks, H. B. Schlegel, G. E. Scuseria, M. A. Robb, J. R. Cheeseman, G. Scalmani, V. Barone, B. Mennucci, G. A. Petersson, et al. Gaussian 09, Revision D.01; Gaussian, Inc., Wallingford CT, 2013.

[25] A.D. Becke, Density-Functional Exchange-Energy Approximation With Correct Asymptotic Behavior. Phys. Rev. A. 38 (1988) 3098–3100.

[26] A.D. Becke, Density-Functional Thermochemistry. III. The Role Of Exact Exchange, J. Chem. Phys. 98 (1993) 5648-5652.

[27] C. Lee, W. Yang, R.G. Parr, Development of the Colle-Salvetti Correlation-Energy Formula Into a Functional of the Electron Density, Phys. Rev. B 37 (1988) 785-789.

[28] S.H. Vosko, L. Wilk, M. Nusair, Accurate Spin-Dependent Electron Liquid Correlation Energies For Local Spin Density Calculations: A Critical Analysis, Can. J. Phys. 58 (1980) 1200-1211.

[29] P.J. Stephens, F.J. Devlin, C.F. Chabalowski, M.J. Frisch, Ab Initio Calculation of Vibrational Absorption and Circular Dichroism Spectra Using Density Functional Force Fields, J. Phys. Chem. 98 (1994) 11623-11627

[30] D. Rappoport, F. Furche, Property-Optimized Gaussian Basis Sets For Molecular Response Calculations, J. Chem. Phys. 133 (2010) 134105.

[31] B. Metz, H. Stoll, M. Dolg, Small-Core Multiconfiguration-Dirac–Hartree–Fock-Adjusted Pseudopotentials For Post-d Main Group Elements: Application To PbH and PbO, J. Chem. Phys. 113 (2000) 2563-2569.

[32] D. Feller, The Role of Databases in Support of Computational Chemistry Calculations, J. Comp. Chem. 17 (1996) 1571-1586,.

[33] K.L. Schuchardt, B.T. Didier, T. Elsethagen, L. Sun, V. Gurumoorthi, J. Chase, J. Li, T.L. Windus, Basis Set Exchange: A Community Database for Computational Sciences, J. Chem. Inf. Model. 47 (2007) 1045-1052.

[34] D. McQuarrie, J. Simon, Molecular Thermodynamics; University Science Books, Mill Valley Ca, 1999.

[35] E. Baudet, C. Cardinaud, A. Girard, E. Rinnert, K. Michel, B. Bureau, V. Nazabal, Structural analysis of RF sputtered Ge-Sb-Se thin films by Raman and X-ray photoelectron spectroscopies, J. Non-Cryst. Solids 444 (2016) 64-72.

[36] E. Baudet, C. Cardinaud, R. Boidin, A. Girard, J. Gutwirth, P. Němec, V. Nazabal, X-Ray photoelectron spectroscopy analysis of Ge–Sb–Se pulsed laser deposited thin films, J. Am. Ceram. Soc. 2018 (in press). https://doi.org/10.1111/jace.15512

[37] L. Pauling, The Nature of the Chemical Bond, Cornell Univ. Press, Ithaca, 1960.

[38] A. Harvey et al., Preparation of gallium sulfide nanosheets by liquid exfoliation and their application as hydrogen evolution catalysts, Chem. Mater. 27, *9* (2015) 3483-3493.

[39] P. Masselin, D. Le Coq, A. Cuisset, E. Bychkov, Spatially Resolved Raman Analysis of Laser Induced Refractive Index Variation in Chalcogenide Glass, Optical Mat. Express 2 (2012) 1768-1775.

[40] I. Pethes, V. Nazabal, R. Chahal, B. Bureau, I. Kaban, S. Belin, P. Jovari, Local motifs in GeS_2-Ga_2S_3 glasses, J. Alloys Compd. 673 (2016) 149-157.

[41] A. Gheorghiu, I. Lampre, S. Dupont, C. Senemaud, M. A. El-Idrissi Raghni, P. E. Lippens, J. Olivier-Fourcade, Electronic structure of chalcogenide compounds from the system Tl_2S-Sb_2S_3 studied by XPS and XES, J. Alloys Compd. 228 (1995) 143.

[42] J. Ibáñez, J.A. Sans, C. Popescu, J. López-Vidrier, J.J. Elvira-Betanzos, V.P. Cuenca-Gotor, O. Gomis, F.J. Manjón, P. Rodríguez-Hernández, A. Muñoz, Structural, Vibrational, and Electronic Study of Sb_2S_3 at High Pressure, J. Phys. Chem. C 120 (2016) 10547−10558.

[43] A. Kyono, A. Hayakawa, M. Horiki, Selenium Substitution Effect on Crystal Structure of Stibnite (Sb_2S_3), Phys. Chem. Minerals 42 (2015) 475–490.

[44] P. Bayliss, W. Nowacki, Refinement of the Crystal Structure of Stibnite Sb_2S_3. Z. Kristallogr, 135 (1972) 308-315.

[45] Zh. Li, Ch. Lin, G. Qu, Q. Nie, T. Xu, Sh. Dai, Phase Separation in Nonstoichiometry Ge–Sb–S Chalcogenide Glasses, J. Am. Ceram. Soc. 97 (2014) 793–797.

[46] K. Miyauchi, J. Qiu, M. Shojiya, Y. Kawamoto, N. Kitamura, Structural Study of GeS_2 Glasses Permanently Densified Under High Pressures up to 9 GPa, J. Non-Cryst. Solids 279 (2001) 186-195.

[47] R. Vahalova, L. Tichy, M. Vlcek, H. Ticha, Far Infrared Spectra and Bonding Arrangement in Some Ge-Sb-S Glasses, Phys. Stat. Sol. A 181 (2000) 199-209.

Figure Captions

Fig. 1. Fitting of Ge 3*d* , Ga 3*d*, and Sb 4*d* core level XPS spectra for the investigated sulfide glasses (dashed lines correspond to best fit doublet components, thick solid line to the experimental XPS spectrum and thin solid line to the fitted curve).

Fig. 2. Fitting of S 2*p* core level XPS spectra for the investigated glasses (dashed lines correspond to best fit doublet components, thick solid line to the experimental XPS spectrum and thin solid line to the fitted curve).

Fig. 3. Raman spectra of the investigated glasses and calculated strongest Raman-active modes of CS [$GeS_{4/2}$]tetrahedra G1 (symmetric stretch 329.54 cm^{-1}, activity 79 a.u.; and asymmetric stretch 382.11 cm^{-1}, activity 18 a.u.); ES [$GeS_{4/2}$] tetrahedra G2 (symmetric stretch 361.67 cm^{-1}, activity 88 a.u.; asymmetric stretch 392.55 cm^{-1}, activity 28 a.u.; and symmetric stretch 424.87 cm^{-1}, activity 15 a.u.); CS [$SbS_{3/2}$] pyramids S1 (symmetric stretch 306.02 cm^{-1}, activity 16 a.u.; and 326.45 cm^{-1}, activity 77 a.u.; and asymmetric stretch 310.98 cm^{-1}, activity 22 a.u.); ES [$SbS_{3/2}$] pyramids S2 (symmetric stretch 310.81 cm^{-1}, activity 16 a.u.; 321.66 cm^{-1}, activity 36 a.u.; and 349.74 cm^{-1}, activity 46 a.u.); CS [$GeS_{4/2}$]-[$SbS_{3/2}$] tetrahedra and pyramids GS1 (symmetric stretch 336.63 cm^{-1}, activity 98 a.u.; and asymmetric stretch 323.55 cm^{-1}, activity 20 a.u.); ES [$GeS_{4/2}$]-[$SbS_{3/2}$] tetrahedra and pyramids GS2 (breathing 353.63 cm^{-1}, activity 65 a.u.; and asymmetric stretch 318.06 cm^{-1}, activity 22 a.u.).

Table 1. Best fit values of characteristic parameters of Ge 3*d* (3$d_{5/2}$ component) core level peaks (the analyzed core level is written in a bold font; *BE* and *fwhm* values are in eV, *A* values are in %).

core level	(S)$_2$>**Ge<**(S)$_2$ ES			(S)$_2$>**Ge<**(S)$_2$ CS			(S)$_3$≡**Ge-**(Ge,Sb,Ga)		
composition	*BE*	*fwhm*	*A*	*BE*	*fwhm*	*A*	*BE*	*fwhm*	*A*
$Ge_{33}S_{67}$	31.34	0.80	14	30.81	0.68	81	30.16	0.85	5
$Ge_{25}Ga_5S_{70}$	31.32	0.82	11	30.80	0.81	87	29.72	0.99	2
$Ge_{25}Sb_5S_{70}$	31.37	0.85	8	30.87	0.81	84	30.31	0.90	8
$Ge_{25}Sb_{10}S_{65}$	31.35	0.85	18	30.83	0.76	72	30.47	0.90	10
$Ge_{20}Sb_{15}S_{65}$	31.30	0.85	23	30.94	0.87	64	30.55	0.84	13

Table 2. Best fit values of characteristic parameters of Sb 4*d* and Ga 3*d* ($d_{5/2}$ components) core level peaks (the analyzed core level is written in bold font; *BE* and *fwhm* values are in eV, *A* values are in %).

core level	$(S)_2>$**Sb**-S ES or $(S)_2>$**Sb**$\equiv(S)_3$			$(S)_2>$**Sb**-S CS			$(S)_2>$**Sb**-(Sb,Ge)			1) $(S)_3\equiv$**Ga**-S 2) $(S)_3\equiv$**Ga**-Ge(Ga)		
composition	*BE*	*fwhm*	*A*	*BE*	*fwhm*	*A*	*BE*	*fwhm*	*A*	*BE*	*fwhm*	*A*
$Ge_{25}Ga_5S_{70}$										1) 19.83	0.90	51
										2) 19.54	0.90	49
$Ge_{25}Sb_5S_{70}$				33.20	0.92	100						
$Ge_{25}Sb_{10}S_{65}$	33.99	1.14	10	33.19	0.87	87	31.39	0.75	3			
$Ge_{20}Sb_{15}S_{65}$	34.15	1.44	10	33.19	0.95	85	31.07	0.80	5			

Table 3. Best fit values of characteristic parameters of S 2*p* (2$p_{3/2}$ component) core level peaks (the analyzed core level is written in bold font; *BE* and *fwhm* values are in eV, *A* values are in %).

core level	S-**S**-S			S-**S**-(Sb,Ge) or S_2			(Sb,Ge)-**S**-(Ge,Sb)			Ga-**S**-Ga		
	BE	*fwhm*	*A*	*BE*	*fwhm*	*A*	*BE*	*fwhm*	*A*	*BE*	*fwhm*	*A*
composition												
$Ge_{33}S_{67}$				162.23	1.52	4	161.65	0.79	96			
$Ge_{25}Ga_5S_{70}$				162.29	1.30	31	161.67	0.93	66	159.25	0.98	3
$Ge_{25}Sb_5S_{70}$	163.03	0.87	4	161.85	1.22	42	161.60	0.97	54			
$Ge_{25}Sb_{10}S_{65}$	163.06	0.89	5				161.65	1.01	95			
$Ge_{20}Sb_{15}S_{65}$	163.07	0.84	4	161.98	0.73	5	161.54	1.19	91			

Table 4. Results of thermochemical calculations for face-shared (FS) vs edge-shared (ES) configurations. The uncertainties in the calculations are about $5 \cdot 10^{-20}$ J.

Reaction	ΔE_{SCF} ($\cdot 10^{-20}$ J)	$\Delta E_{SCF+Zero\ pt}$ ($\cdot 10^{-20}$ J)	$\Delta E_{Thermal}$ ($\cdot 10^{-20}$ J) T=25 °C	ΔH ($\cdot 10^{-20}$ J) T=25 °C	ΔG ($\cdot 10^{-20}$ J) T=25 °C
(4.1) $Ga_2S_3 + SH_2 \rightarrow Ga_2S_4H_2$	-79.0	-77.5	-77.5	-77.9	-70.5
(4.2) $GaGeS_4H + SH_2 \rightarrow GaGeS_5H_3$	-51.5	-50.3	-50.2	-50.6	-43.4
(4.3) $GaSbS_3 + SH_2 \rightarrow GaSbS_4H_2$	-34.0	-33.1	-32.8	-33.2	-27.0
(4.4) $Ge_2S_5H_2 + SH_2 \rightarrow Ge_2S_6H_4$	-27.8	-26.6	-26.5	-26.9	-19.6
(4.5) $Sb_2S_3 + SH_2 \rightarrow Sb_2S_4H_2$	-10.7	-10.1	-9.6	-10.0	-4.5
(4.6) $SbGeS_4H + SH_2 \rightarrow SbGeS_5H_3$	-17.1	-16.1	-15.8	-16.2	-9.9

Table 5. Results of thermochemical calculations for edge-shared (ES) vs corner-shared (CS) configurations. The uncertainties in the calculations are about $5{\cdot}10^{-20}$ J.

Reaction	ΔE_{SCF} ($\cdot 10^{-20}$ J)	$\Delta E_{SCF+Zero\ pt}$ ($\cdot 10^{-20}$ J)	$\Delta E_{Thermal}$ ($\cdot 10^{-20}$ J) T=25 °C	ΔH ($\cdot 10^{-20}$ J) T=25 °C	ΔG ($\cdot 10^{-20}$ J) T=25 °C
(5.1) $Ga_2S_4H_2 + SH_2 \rightarrow Ga_2S_5H_4$	-5.64	-4.77	-4.45	-4.86	1.24
(5.2) $GaGeS_5H_3 + SH_2 \rightarrow GaGeS_6H_5$	-4.16	-3.34	-2.97	-3.38	2.97
(5.3) $GaSbS_4H_2 + SH_2 \rightarrow GaSbS_5H_4$	-3.16	-2.47	-2.04	-2.45	3.14
(5.4) $Ge_2S_6H_4 + SH_2 \rightarrow Ge_2S_7H_6$	-2.64	-1.82	-1.44	-1.86	4.54
(5.5) $Sb_2S_4H_2 + SH_2 \rightarrow Sb_2S_5H_4$	-2.44	-1.76	-1.37	-1.79	4.57
(5.6) $SbGeS_5H_3 + SH_2 \rightarrow SbGeS_6H_5$	-2.79	-2.09	-1.61	-2.02	3.92

Table 6. Results of thermochemical calculations for metal-metal bonds vs corner-shared (CS) and S-S bridge-shared units. The uncertainties in the calculations are about $5 \cdot 10^{-20}$ J.

Reaction	ΔE_{SCF} ($\cdot 10^{-20}$ J)	$\Delta E_{SCF+Zero\ pt}$ ($\cdot 10^{-20}$ J)	$\Delta E_{Thermal}$ ($\cdot 10^{-20}$ J) T=25 °C	ΔH ($\cdot 10^{-20}$ J) T=25 °C	ΔG ($\cdot 10^{-20}$ J) T=25 °C
(6.1) $Ge_2S_6H_6$ + $Sb_2S_5H_4$ → $Sb_2S_4H_4$ + $Ge_2S_7H_6$	-1.73	-1.55	-1.58	-1.58	-1.44
(6.2) $SbGeS_5H_5$+ $Sb_2S_5H_4$ → $Sb_2S_4H_4$ + $SbGeS_6H_5$	-1.60	-1.63	-1.52	-1.52	-2.01
(6.3) $SbGeS_5H_5$+ $Ge_2S_7H_6$ → $Ge_2S_6H_6$ + $SbGeS_6H_5$	0.13	-0.08	0.06	0.06	-0.57
(6.4) $Sb_2S_4H_4$ + $Sb_2S_6H_4$ → 2 $Sb_2S_5H_4$	-12.37	-12.21	-12.44	-12.44	-11.64
(6.5) $Ge_2S_6H_6$ + $Sb_2S_6H_4$→ $Ge_2S_7H_6$ + $Sb_2S_5H_4$	-14.10	-13.76	-14.02	-14.02	-13.07
(6.6) $Ge_2S_6H_6$ + $Ge_2S_8H_6$→ 2 $Ge_2S_7H_6$	-14.79	-14.31	-14.65	-14.65	-13.01
(6.7) $SbGeS_5H_5$+ $Sb_2S_6H_4$ → $SbGeS_6H_5$ + $Sb_2S_5H_4$	-13.98	-13.84	-13.96	-13.96	-13.64
(6.8) $Ge_2S_7H_6$ + $Sb_2S_6H_4$→ $Ge_2S_8H_6$ + $Sb_2S_5H_4$	0.69	0.54	0.63	0.63	-0.07
(6.9) $SbGeS_6H_5$+ $Sb_2S_6H_4$→ $SbGeS_7H_5$ + $Sb_2S_5H_4$	1.13	1.17	1.03	1.03	1.38

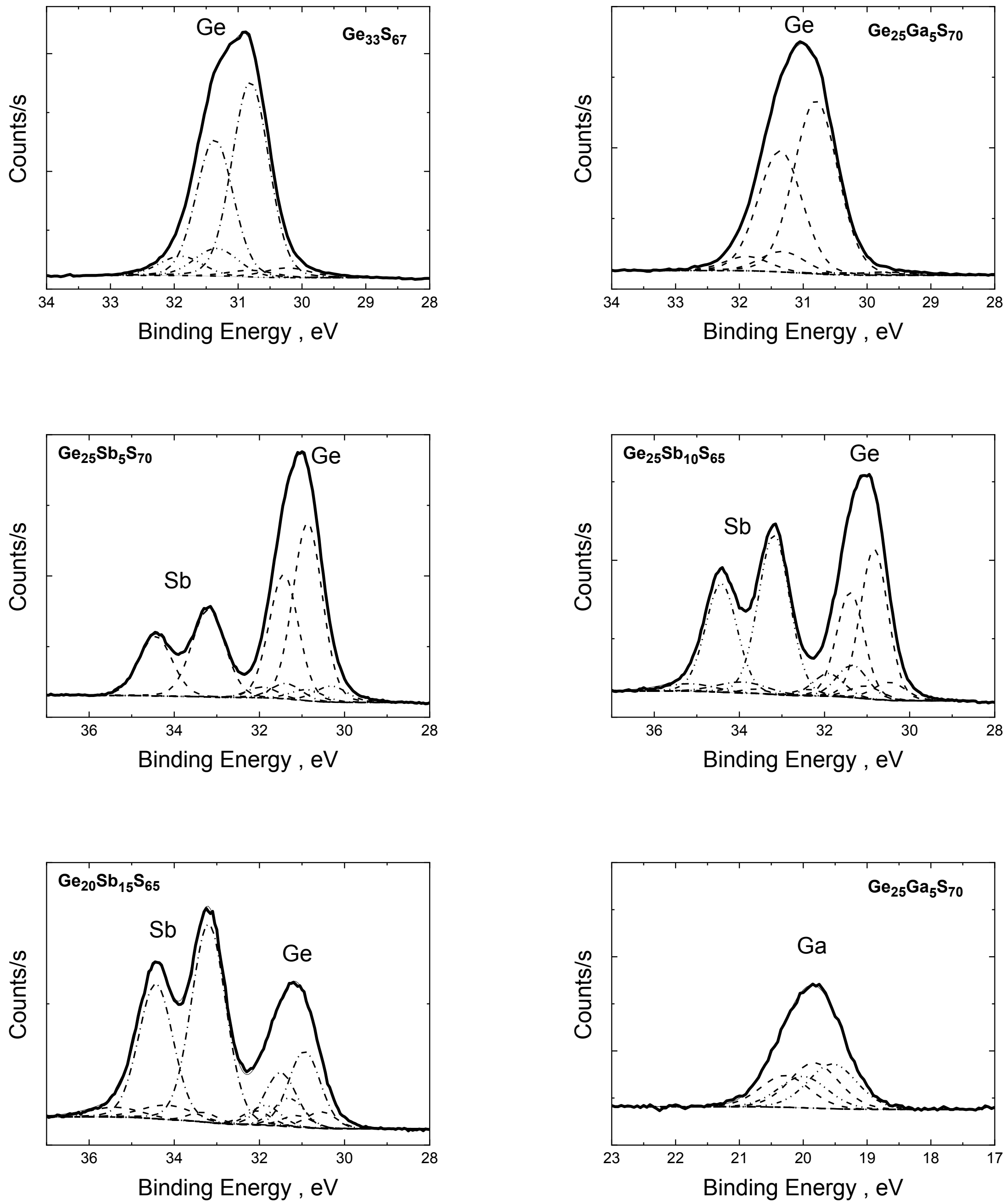

Ge
$Ge_{33}S_{67}$
Counts/s
34 33 32 31 30 29 28
Binding Energy , eV
Ge
$Ge_{25}Ga_5S_{70}$
Counts/s
34 33 32 31 30 29 28
Binding Energy , eV
$Ge_{25}Sb_5S_{70}$
Sb
Ge
Counts/s
36 34 32 30 28
Binding Energy , eV
$Ge_{25}Sb_{10}S_{65}$
Sb
Ge
Counts/s
36 34 32 30 28
Binding Energy , eV
$Ge_{20}Sb_{15}S_{65}$
Sb
Ge
Counts/s
36 34 32 30 28
Binding Energy , eV
$Ge_{25}Ga_5S_{70}$
Ga
Counts/s
23 22 21 20 19 18 17
Binding Energy , eV

Figure 1.

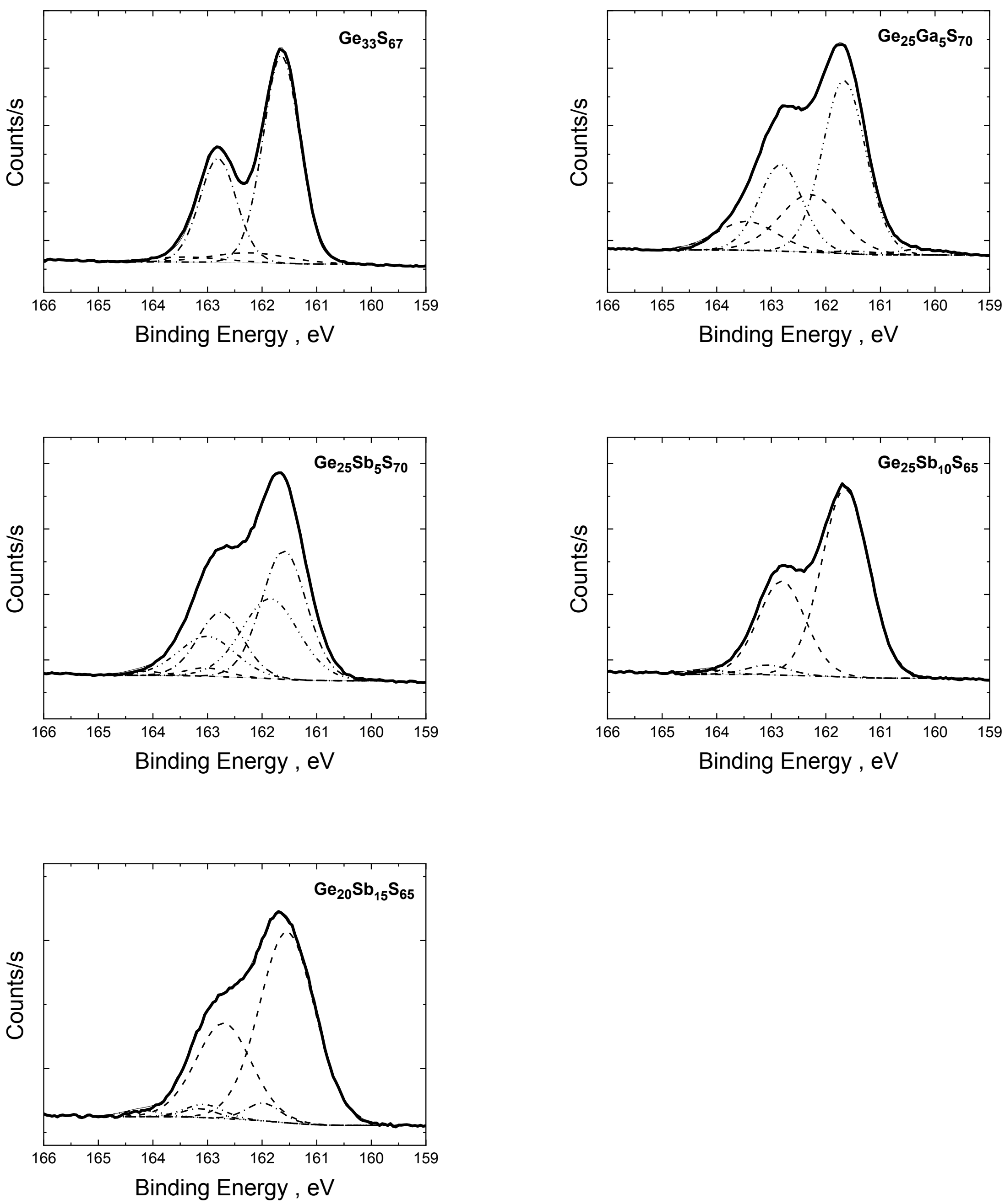

$Ge_{33}S_{67}$
$Ge_{25}Ga_{5}S_{70}$
$Ge_{25}Sb_{5}S_{70}$
$Ge_{25}Sb_{10}S_{65}$
$Ge_{20}Sb_{15}S_{65}$
Counts/s
166 165 164 163 162 161 160 159
Binding Energy , eV

Figure 2.

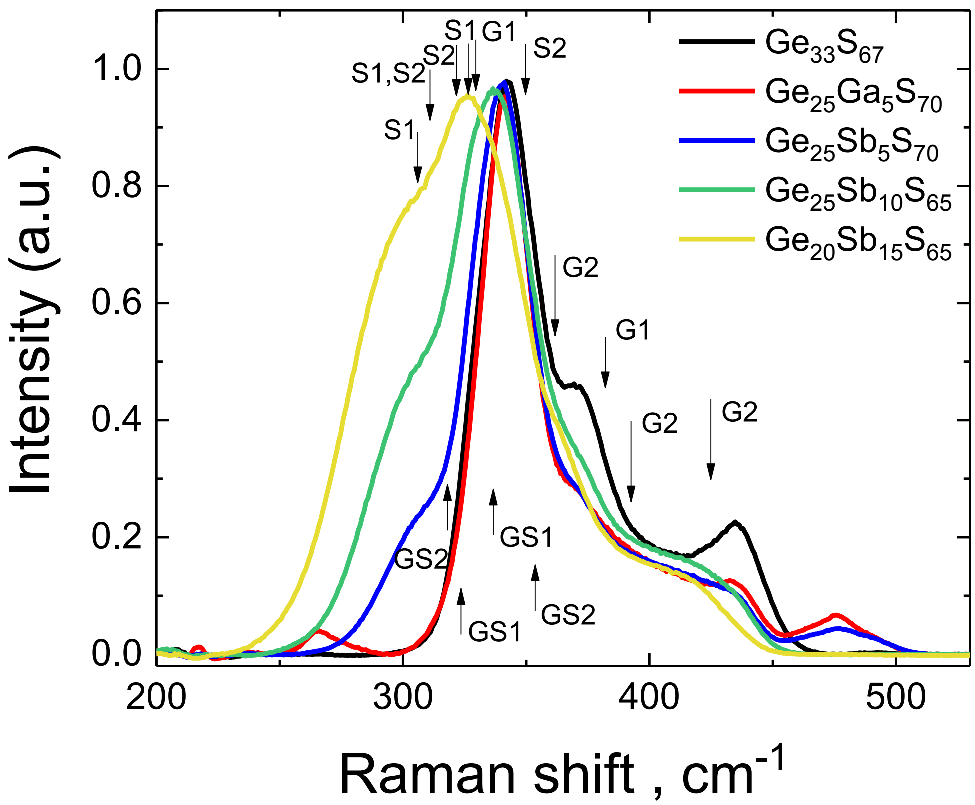

Intensity (a.u.)
Raman shift , cm-1
Ge33S67
Ge25Ga5S70
Ge25Sb5S70
Ge25Sb10S65
Ge20Sb15S65
S1,S2
S2
S1
G1
S2
S1
G2
G1
G2
G2
GS2
GS1
GS1
GS2

Figure 3.